ACS ES&T Engineering

pubs.acs.org/estengg

Article

# Ultrafast Carbothermal Process of Municipal Solid Waste Incineration Fly Ash for Purification and Valuable Elements Recovery

Tengfei Zheng, Huizhen Wang, Rencheng Zhou, Xinye Wang,* Changqi Liu, Hao Xie, Feifei Zhou, and Haining Meng*

Cite This: https://doi.org/10.1021/acsestengg.4c00354

Read Online



**ABSTRACT:** Municipal solid waste incineration fly ash (MSWI FA), containing heavy metals and dioxins that can migrate and accumulate in the biosphere, is harmful to human health and the environment. Thermal treatment can effectively purify MSWI FA, but it is not widely used due to high energy consumption and long calcination time. Herein, we report an ultrafast carbothermal process to heat ash to 3600 °C within 0.03 s for FA purification and valuable elements recovery. After one time of ultrafast heating, 99.91% of the dioxins were removed, and the purified ash met the leaching standards. After three ultrafast heating cycles, the removal efficiencies of heavy metals were up to 71% for Zn, 86% for Pb, 71% for Cu, 62% for As, 100% for Hg, 93% for Cd, and 70% for Ni. The ultrafast carbothermal process also promoted chlorine removal by an ash washing process due to the decomposition of CaClOH. The condensate of volatiles was a good urban mining resource, higher than the minimum industrial grade of ore deposit. Compared with the traditional carbothermal treatment, it consumed only 1/110 of energy and needed 1/1920 of the furnace volume. The ultrafast carbothermal process provides an efficient and environmentally friendly way for FA purification and valuable elements recovery.

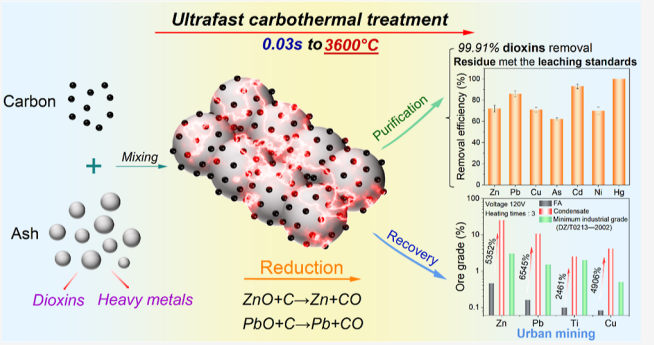


**KEYWORDS:** *MSWI fly ash, ultrafast carbothermal process, purification, recovery*



## 1. INTRODUCTION

Incineration, as an important means of disposing municipal solid waste (MSW), can efficiently reduce the volume by 85%−90% and the mass by 60%−90%, accompanied by the production of electrical or thermal energy.[1] MSW incineration (MSWI) is popular particularly in densely populated countries, where urban land resources become scarce increasingly. In 2021, 62% of unresourced MSW was incinerated in China,[2] while 90% and 38% in Japan[3] and the European Union, respectively.[4] Even in the United States[5] where the population is not dense, incinerated MSW accounted for 15% (Figure S1). However, incineration produces highly toxic fly ash (FA), which is classified as hazardous waste worldwide for heavy metals and dioxins inside.[6−8] The annual production of MSWI FA in China was estimated to be as high as 10 million tons in 2021.

The main way of MSWI FA disposal is landfill after chelation, which weakens the solubility, the mobility, and the toxicity of heavy metals.[9−11] However, the long-term stability has been widely questioned. Du et al. found that lead (Pb) and cadmium (Cd) in the 6 year-old chelator-stabilized FA were 12 and 9.7 times the standard limits, respectively.[12] Therefore, the old landfills pose significant environmental risks. In recent years, the trend has been to replace landfill with cement kilns to deposal MSWI FA in China.[13] Even if the heavy metals are theoretically fixed in cement clinker, their long-term stabilities are not clear yet. Consequently, for either landfill or resource utilization, heavy metals are the biggest obstacle to the harmless disposal of FA. Compared to fixing heavy metals, removing them should be the safest method to completely eliminate the environmental risks arising from heavy metals release.

Thermal separation and wet separation are the main methods of heavy metals removal from FA.[14] Wet separation uses acid washing to dissolve heavy metals from ash into solution.[15] Its operation cost is high for chemicals consumption, wastewater treatment, and wet product drying.[16]

Received: June 18, 2024
Revised: October 2, 2024
Accepted: October 3, 2024

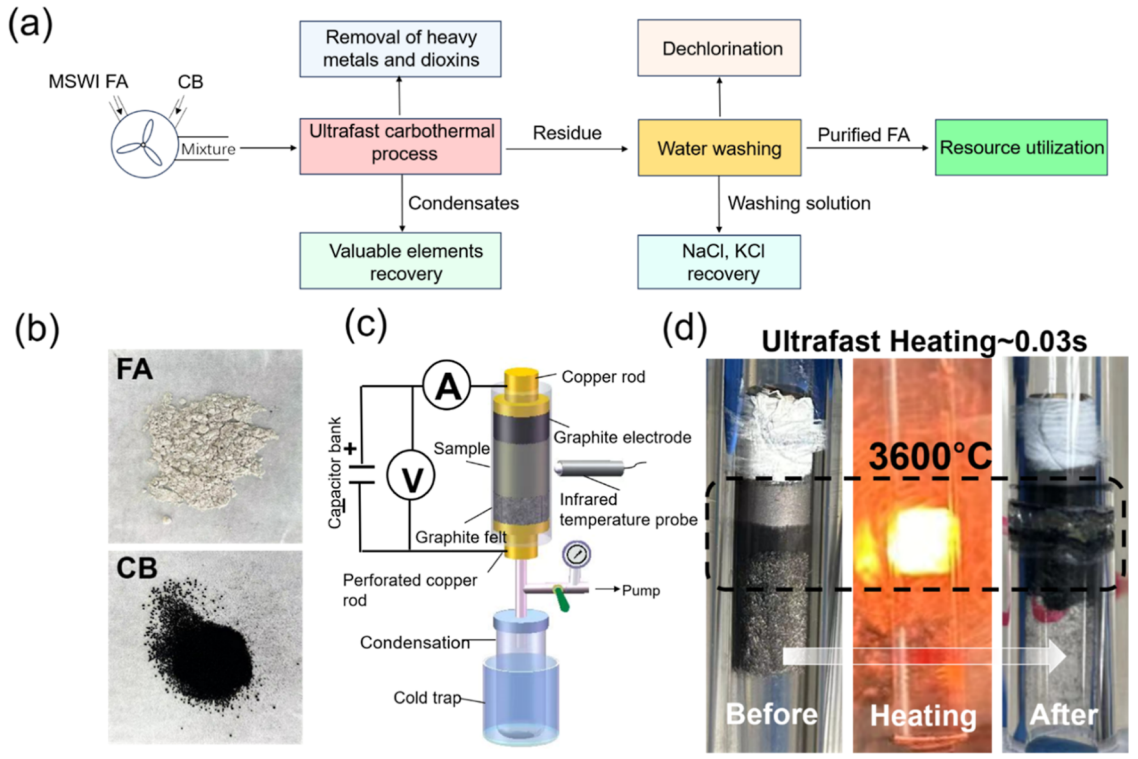


**Figure 1.** Overall process of MSWI FA pretreatment and schematic of the ultrafast carbothermal process. (a) Pretreatment process for resource utilization of MSWI FA. (b) Physical image of MSWI FA and conductive carbon (Cabot, Black Pearls 2000) CB. (c) Reactor diagram of the ultrafast carbothermal process. (d) Physical image of the sample heating.

Thermal separation uses high temperature to volatilize heavy metals from FA to flue gas, which is cooled then to condense and collect heavy metals.[17] Compared to the wet process, the thermal process is simpler and therefore has more application prospects. However, its operation cost is still too high for industrial applications due to the high energy consumption of ash heating. Therefore, how to lower the heating temperature has become the hot issue of thermal separation research. Adding chlorinating agents to FA is effective in lowering the heating temperature. Various chlorinating agents have been studied such as HCl, $Cl_2$, PVC, $CaCl_2$, $MgCl_2$, NaCl, etc.[18,19] However, it causes two other issues of more chlorides in ash and more dioxins in flue gas.[20,21] Recently, Lane et al. proposed reduction thermal separation by 10% $H_2$, which lowered the heating temperature to 1000 °C without those two issues theoretically, but it failed to remove copper (Cu).[22] Regardless of what additive is used, the temperature of thermal separation should be higher than at least the melting point of heavy metal compounds, preferably the boiling point. Therefore, the heating temperatures in previous studies were never below 750 °C.[22]

In fact, the high energy consumption is caused not only by high temperatures but also by the heating duration, which was up to 2 h in previous studies on MSWI FA thermal treatment. No research has been found yet on how to shorten this duration. In this study, we tried to shorten it from hours to seconds by an ultrafast electrothermal process named flash Joule heating (FJH), which has already been applied in material synthesis,[23] material activation,[24] waste management,[25−28] and graphene production.[29] First, the heating characteristics of FA during the ultrafast carbothermal process were investigated for the optimal heating parameters and the heating mechanisms. Then, the effect of ultrafast carbothermal process was evaluated on ash purification, valuable metal element recovery, and chlorine removal. After that, the condensates of volatiles were analyzed by X-ray photoelectron spectroscopy (XPS) and energy-dispersive X-ray spectroscopy (EDS) for the migration and transformation mechanisms of heavy metals. Furthermore, by comparing the X-ray diffraction (XRD) patterns of FA before and after heating, we investigated the mechanism by which the ultrafast carbothermal process enhances the dissolution of chlorine during the FA washing process. Finally, the energy consumption and reactor size of the ultrafast carbothermal process were calculated and they were much smaller than that of traditional thermal treatment.

## 2. EXPERIMENTAL SECTION

**2.1. Chemicals and Materials.** The MSWI FA was collected from an MSWI plant in Jiangsu, China. Carbon black (CB) is used as the conductive additive. Detailed descriptions of FA, CB, and their mixture for heating are provided in the Supporting Information (Text S1).

**2.2. Overall Process of MSWI FA Pretreatment.** This study proposes a pretreatment process for the resource utilization of FA (Figure 1d). Initially, the ultrafast carbothermal process generates high temperatures that remove heavy metals and dioxins from FA, recovering condensates enriched with valuable elements. Subsequently, the residue is washed to remove chlorine, producing a wash liquid rich in NaCl and KCl. Through this pretreatment, the FA can be further used as a resource.

**2.3. Ultrafast Carbothermal Experiments.** The experimental device is composed of a reaction tube, electrodes, a capacitor bank, an infrared temperature probe, and a cold trap, as shown in Figure 1. The mixture of FA and CB (Figure 1a) was loaded inside the quartz tube between two electrodes. The


https://doi.org/10.1021/acsestengg.4c00354
ACS EST Engg. XXXX, XXX, XXX−XXX

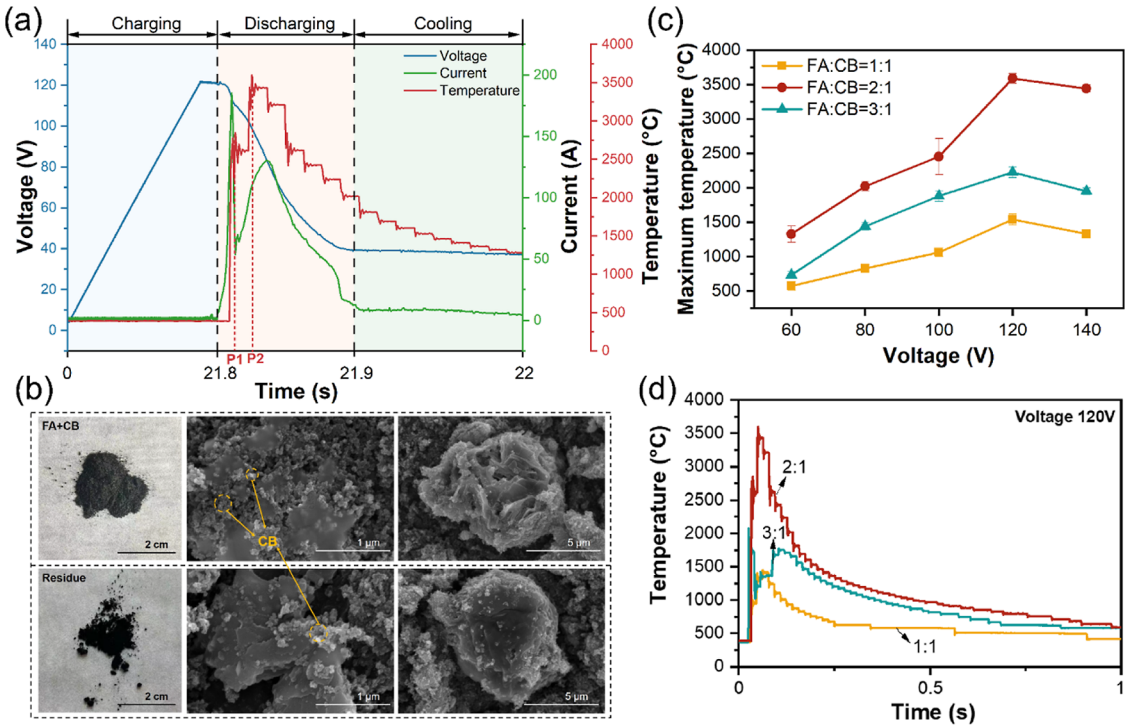


**Figure 2.** Discharge characteristics and heating effect ultrafast carbothermal process. (a) Changes in voltage, current, and temperature over time during the ultrafast carbothermal process at the FA/CB of 2:1 and the initial voltage of 120 V, where P1 and P2 are the corresponding time of two temperature peaks. (b) SEM images of the sample before and after the ultrafast carbothermal process at the initial voltage of 120 V. (c) Maximum temperatures at three mass ratios and five initial voltages from 60 to 140 V. (d) Temperatures at three mass ratios and initial voltage 120 V during the whole heating stage.

mass of the sample processed in a single process is 0.1 g, and according to the mass ratio of ash to carbon, three types of ash carbon mixtures were prepared for ultrafast carbon thermal experiments.

The cathode was made of a copper tube with graphite felt at the front end to block the reaction material and facilitate the gas diffusion. The anode was made of a copper rod with the graphite powder (described in Supporting Information Text S12) at the front end to block the reaction material and gas. The resistance of the sample was adjusted by the compression of the sample by two electrodes. The heating power was supplied by a capacitor bank with a total capacitance of 90 mF. After vacuuming, the high-voltage discharge of the capacitor bank heated the sample in 1 s to high temperature (Figure 1c), which was measured by an infrared temperature probe with millisecond-level data acquisition. Such a high temperature enables the evaporation of heavy metals, which were captured by condensation in a cold trap that was soaked in liquid nitrogen. Concentrated nitric acid was used to rinse the inner walls of the condenser, ensuring that the condensate fully dissolved without manual removal. The data presented here represent the average results of three parallel experiments. The steps for implementing multiple heating cycles include charging, discharging, and adjusting the resistance. Detailed explanations are provided in Text S15.

**2.4. Water Washing Experiments.** Water washing was used to remove chlorine from the ash. Using a magnetic stirrer, 10 g of noncarbon residues was combined with 30 mL of deionized water in a 250 mL Erlenmeyer flask, agitating at a rate of 500 rpm. The detailed dissolution fraction of chlorine ($W_{Cl\text{-}d}$) was calculated following eq S1.

**2.5. Analytical Methods.** The details for the analytical methods are provided in Texts S3–S6.

## 3. RESULTS AND DISCUSSION

**3.1. Effect of Heating and Characteristics of Discharge during the Ultrafast Carbothermal Process.** Discharge and heating of three samples during the ultrafast carbothermal process were investigated at the discharge voltages from 60 to 140 V. A typical ultrafast carbothermal process (Figure 2a) comprised charging, discharging, and cooling phases. After charging for 21.8 s to reach 120 V, the discharge was finished within 0.1 s mainly and then was maintained at 40 V. During the discharge stage, there were two peaks of current and temperature. The first peak was narrow and around 180 A at 0.006 s, resulting in the sharp rise of temperature to around 2700 °C. The second peak was broad and around 130 A at 0.03 s, resulting in the continuous rise of temperature to around 3600 °C. The traditional thermal treatment of ash in plasma or resistance furnace produces the total melting of ash, which needs water quenching for cooling.[25] During the ultrafast carbothermal process at the initial voltage 120 V, the ash was heated to approximately 3600 °C within 0.03 s and cooled to 400 °C within 0.2 s (Figure 2a), so the residue could be cooled naturally without water quenching. No significant melting, even no significant sintering, was found in the SEM image of residue, but only slight melting was observed in the ash particle surface (Figure 2b).

During the thermal treatment of the FA, temperature is one of the significant factors affecting the purification of FA. Therefore, the maximum temperature reached during the ultrafast carbothermal process was used as the evaluating


https://doi.org/10.1021/acsestengg.4c00354
ACS EST Engg. XXXX, XXX, XXX−XXX

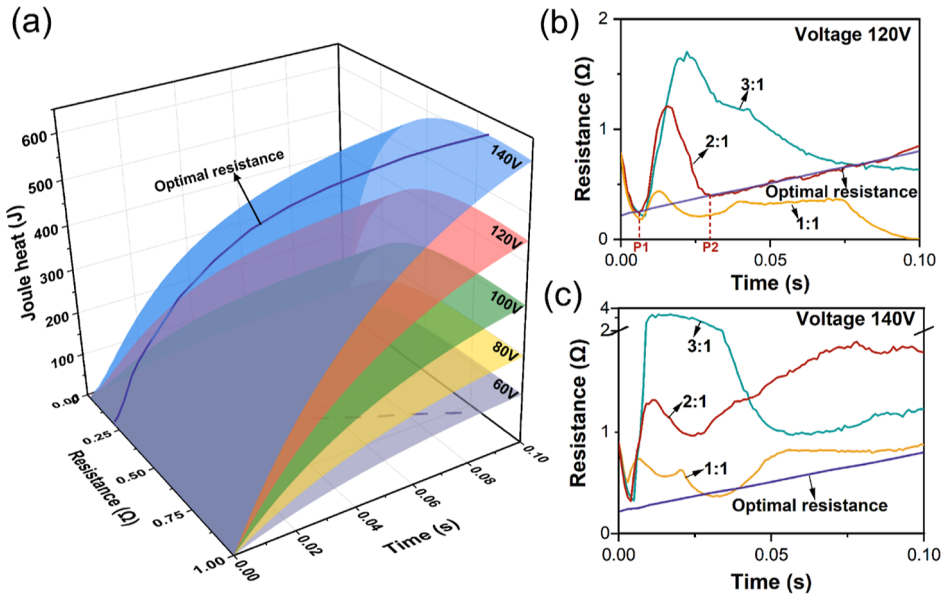


**Figure 3.** Mechanism for selecting the initial voltage and the optimal ash-to-carbon ratio. (a) Theoretical changes in accumulated heat of sample over time and sample resistance at five initial voltages from 60 to 140 V. Changes in actual sample resistance and theoretical optimal resistance over time at (b) 120 V and (c) 140 V.

indicator for the heating effect. As shown in Figure 2c, the FA to CB mass ratio of 2:1 and the initial voltage of 120 V were the optimum parameters for ultrafast carbothermal process.

**3.2. Mechanisms of Choice Are the Initial Voltage and Optimal Ash to Carbon Ratio.** Although the samples with different FA to CB mass ratios had the same initial resistances of 0.78 Ω, their heating temperatures were different. The sample with the FA to CB mass ratio of 2:1 always had the highest temperature during the whole heating stage (Figure S2). To further understand the reasons for the optimal ratio, the variation of accumulated heat (Figure 3a) of the sample over time was calculated under the assumption of constant resistance because it was the direct factor that determined the sample temperature. It is evident that the accumulated heat of sample increased with the increase of voltage and time. However, the resistance of sample showed some complexity on the accumulated heat. The theoretical optimal resistance corresponding to the maximum heat increased with time almost in a linear relationship (Figure 3a) and was independent of the voltage. The optimal resistance calculation during the heating period is detailed in Text S7. The actual resistances of samples also changed over time but were fluctuated and did not match the optimal resistance (Figure 3b). In contrast, the resistance of the sample with the FA to CB mass ratio of 2:1 was the closest to the optimal resistance. When the actual resistance was consistent with the theoretical optimal resistance, the temperature peak was shown. Both two peaks of the sample with the FA to CB mass ratio of 2:1 in Figure 2d follows this rule, proving the correctness of the theoretical calculations. Therefore, the change in sample resistance over time is the decisive factor in the ultrafast heating effect.

The conductivity of the sample is due to the presence of CB, so the resistance of the sample includes the inherent resistance of CB and the contact resistance between carbon particles. During the initial stage of heating, the inherent resistance of CB decreased with increasing temperature because of its inherent physical property, so the downward trends of the samples with three ratios were close. Then, the sharp rise of sample temperature caused the rapid expansion of gas in the sample, resulting in poorer contact between carbon particles and consequently higher contact resistance. The sample with the FA to CB mass ratio of 3:1 contained the least CB; therefore, its contact resistance rose most. On the contrary, the sample with the FA to CB mass ratio of 1:1 had the weakest impact. This conclusion also applies to ash to carbon mass ratios of 1:1 and 3:1. The temperature range of 0−0.1 s in Figure 2d was selected, and it was found that the actual resistance curve intersects with the optimal resistance curve when there is a maximum temperature within 0−0.1 s (Figure S7). Therefore, this conclusion also applies to 1:1 and 3:1.

Theoretically, 140 V brings more Joule heat of the sample than 120 V (Figure 3a). Actually, the maximum temperature was 120 V (Figure 2c). The resistances of samples at 140 V were much higher than that at 120 V, so they further deviated from the optimal value (Figure 3c). It seems that the heating at 140 V instantly produced significant expansion of gas, which was unable to be extracted promptly, so the contact resistance of carbon particles was much higher. The discussion on the temperature differences between the 3:1 and 1:1 ash-to-carbon mass ratios can be found in the Supporting Information, Text S16.

**3.3. Effect of Ultrafast Carbothermal Process on Ash Purification.** The changes in heavy metal removal efficiencies with initial voltage (Figure 4a) agree with those in maximum heating temperature (Figure 2c). At 60−120 V, higher voltage was beneficial for increasing the removal efficiency, but at 140 V, the removal efficiencies were lower. At 120 V, the removal efficiencies of heavy metals were 50% for Zn, 53% for Cu, 61% for Pb, 44% for As, 100% for Hg, 85% for Cd, and 50% for Ni (Figure 4b). The removal rate of Cu is particularly inspiring because Cu has never been removed effectively by thermal reduction of FA in previous researches. He et al.[32] removed 20% of Cu from FA by 2 h carbothermal treatment at 1000 °C. Jacob et al.[33] failed to remove Cu from FA by 1 h calcination at 1130 °C with the atmosphere of 7% $H_2$. Lane et al.[22] removed


https://doi.org/10.1021/acsestengg.4c00354
ACS EST Engg. XXXX, XXX, XXX−XXX

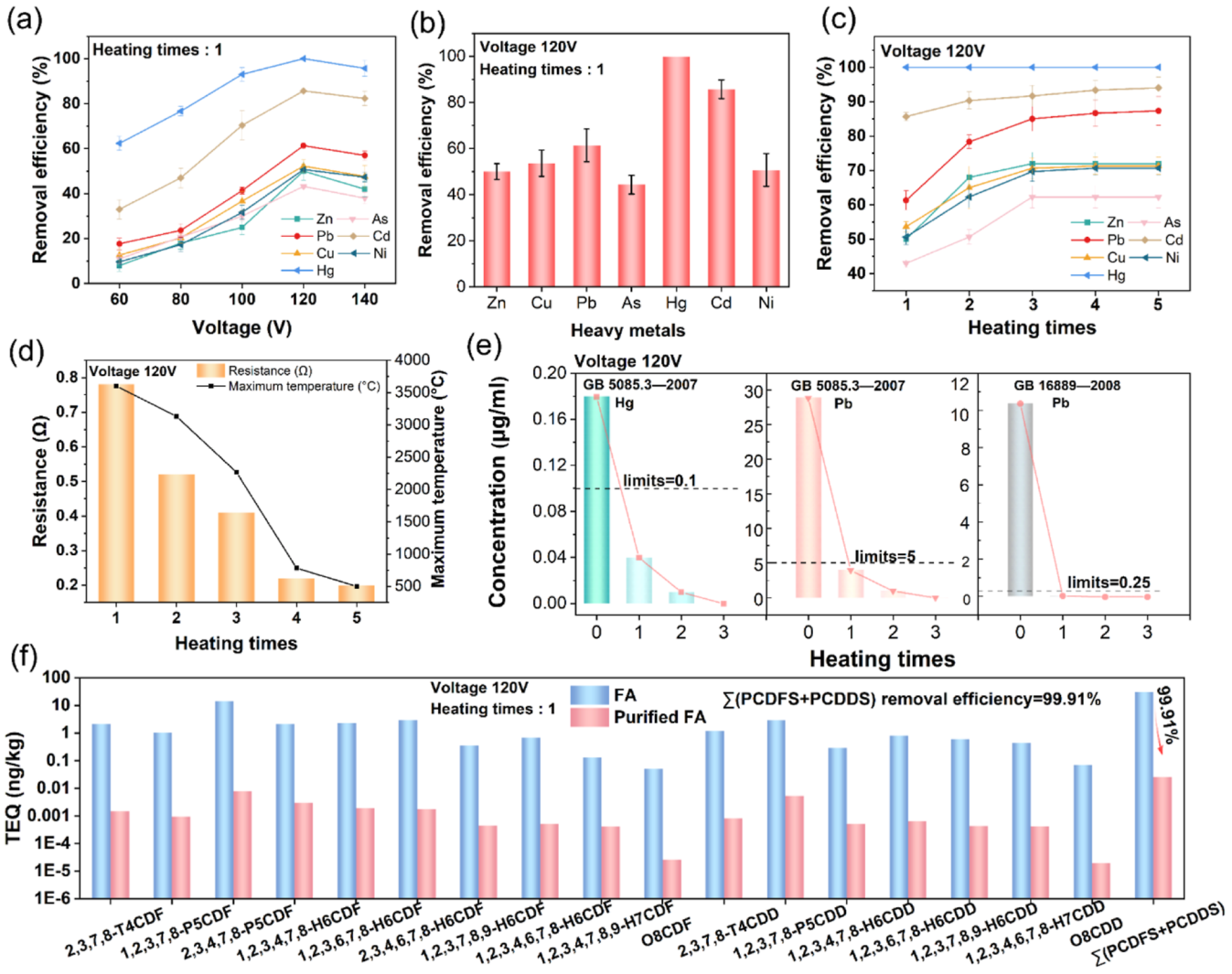


**Figure 4.** Removal effect of heavy metals and dioxins in FA. (a) Removal efficiencies of heavy metals at five initial voltages from 60 to 140 V. (b) Removal efficiency of heavy metals at the initial voltage of 120 V. (c) Removal efficiencies of heavy metals under the heating times from 1 to 5. (d) Changes in resistance and maximum temperature over heating times. (e) Leaching concentrations of Hg and Pb in ash after multiple heating times. Dashed lines represent the concentration limits of Chinese standard. (f) TEQ concentrations of dioxins in ash before and after the ultrafast carbothermal process at the initial voltage of 120 V.

25% of Cu from FA by 0.9 h calcination at 1050 °C with the atmosphere of 10% $H_2$. Therefore, an ultrafast carbothermal process has achieved a breakthrough in separating Cu from FA.

To further increase the removal efficiencies, the sample was heated multiple times, and the results are shown in Figure 4c. After heating three times, the removal efficiencies of heavy metals were increased to 60−100%. The fourth heating could not improve the removal efficiencies anymore because its heating temperature was as low as 782 °C (Figure 4d). After each heating, the resistance of the sample became smaller and deviated from the optimal resistance, especially after the third heating time (Figure 4d). The sample's temperature increased instantaneously during the heating, leading to the production of expansion gas. This resulted in the formation of gaps within the sample after heating, causing an increase in resistance, or, in some cases, even an open circuit. We addressed this by adjusting the electrode spacing to compress the sample. Chen et al. found that nanoparticles are prone to agglomeration during Joule heating.[30] Interestingly, the sample resistance decreases after compression of the electrode, which may be due to the agglomeration of CB. Before heating, the CB was dispersed within the FA, and during high-temperature heating, the CB agglomerated with the expanding gas to form a conductive carbon pathway. Consequently, after each heating, the sample's resistance decreased. The sample temperature is determined by both the voltage and the sample resistance. When the initial voltage remains constant and the resistance decreases, the heating temperature also decreases. The ultrafast carbothermal process not only reduced the heavy metals in ash but also reduced the leaching toxicity of ash. According to the leaching standards of China, the concentrations of Hg and Pb are unqualified in the FA, which consequently cannot be buried in the landfill for MSW (GB 16889-2008) and is classified as hazardous waste (GB 5085.3-2007). After one time of heating, the leaching concentrations of Hg and Pb decreased below both the limits (Figure 4e). The leaching concentrations of other heavy metals in FA after heating are listed in Table S1.

The high temperature treatment of FA for heavy metal removal can remove dioxins as well for volatilization and


https://doi.org/10.1021/acsestengg.4c00354
ACS EST Engg. XXXX, XXX, XXX−XXX

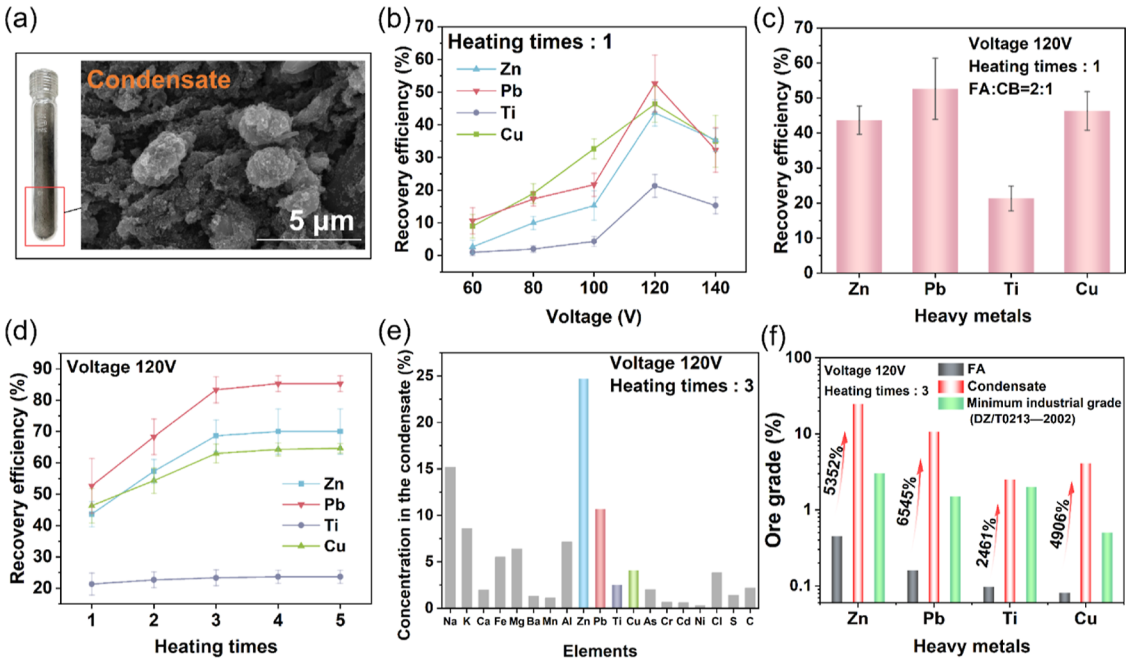


**Figure 5.** Results of elements recovery by condensate collection. (a) Condensate collected in the recovery tube. (b) Recovery efficiencies of heavy metals at five initial voltages from 60 to 140 V. (c) Recovery efficiency of heavy metals at the initial voltage of 120 V. (d) Recovery efficiencies of heavy metals under the heating times from 1 to 5. (e) Concentration of elements in the condensate collected from 3 times of heating at the initial voltage of 120 V. (f) Comparison among the ore grades of FA, condensate, and the lowest industrial requirement for Zn, Pb, Ti, and Cu.

decomposition.[34] After an ultrafast carbothermal process, 99.91% of the dioxins were removed (Figure 4f). The detailed concentration changes of various dioxin substances in ash before and after the ultrafast carbothermal process are shown in the Supporting Information Table S2. The reason for not further analyzing the mechanism of dioxin removal in this study can be found in the Supporting Information (Text S17).

**3.4. Effect of Ultrafast Carbothermal Process on Valuable Elements Extraction.** Most volatilized elements were collected in the condenser tube in the form of microparticles (less than 5 $\mu$m) covered with a large number of nanoparticles (less than 50 nm), as shown in Figure 5a. The sample loss in the recovery system was minimal, and the elemental balance between the residue and the condensate is provided in the Supporting Information, specifically in Text S13 and Figure S10. It has potential commercial value to recover the valuable elements with high concentration in the condensate, such as Zn, Pb, Cu, and Ti. Higher voltage was beneficial for higher recovery efficiency but 140 V was not, so 120 V was the optimal voltage (Figure 5b), which agrees with the changes in maximum heating temperature (Figure 5b). At 120 V, the recovery efficiencies of heavy metals were 44% for Zn, 53% for Pb, 22% for Ti, and 47% for Cu (Figure 5c). Although the Cu and Ti recovered were less than Zn and Pb, their economic values are much higher. As mentioned in Section 3.3, the ultrafast carbothermal process has extracted much more Cu from FA than other reduction thermal treatment. Furthermore, the extraction of Ti was successful as well, which was reported by few studies of FA thermal treatment.

Multiple heating times not only increased the heavy metal removal efficiency but also increased the recovery efficiency. The removal efficiency was used to describe the purification effectiveness of heavy metals in FA, while the recovery efficiency described the effectiveness of recovering valuable elements. The definitions of removal and recovery efficiency are provided in the Supporting Information, Text S8. After three heating times at 120 V, the recovery efficiencies of heavy metals were increased to 68% for Zn, 83% for Pb, 23% for Ti, and 63% for Cu (Figure 5d). The ineffectiveness of more heating is explained in Section 2.3. To evaluate the recovery of valuable elements, it is better to use their concentrations in condensate than the recovery rate of valuable elements in FA. In the condensate collected from 3 heating times at the initial voltage of 120 V, Zn, Pb, Ti, and Cu accounted for 25%, 11%, 2.5%, and 4.1% (Figure 5e), respectively, which were increased by 5352%, 6545%, 2461%, and 4906% (Figure 5f), respectively, compared with their concentrations in the FA. The concentrations of Zn, Pb, and Cu in the condensate were much higher than the requirement of minimum industrial grade (DZ/t0213-2002). The concentrations of Ti met was the requirement as well. Compared to extracting these metals from ores, extracting these metal elements from condensates is considered easier. Because heavy metals mainly exist in the form of chlorides and elemental substances in the condensate as well as soluble salt impurities such as sodium chloride and potassium chloride. Therefore, wet metallurgical technology can be used for heavy metal recovery in condensates. The recovery efficiencies of the other heavy metals in FA are shown in Figure S3. The recovery efficiencies of heavy metals with the mass ratio of FA to CB of 3:1 and 1:1 are shown in Figure S4. The recovery plan for Zn, Pb, and Cu from condensates is detailed in Supporting Information, Text S10. The industrial collection system and description of condensates are provided in Figure S9 and Text S11, respectively.

**3.5. Mechanisms of Migration and Transformation of Valuable Elements.** In FA, Pb species primarily comprises $PbCl_2$ (mp 501 °C and bp 950 °C) and PbO (mp 855 °C and bp 1472 °C). In condensate, PbS (mp 1114 °C and bp 1281 °C) and elemental Pb (mp 327 °C and bp 1740 °C) were


https://doi.org/10.1021/acsestengg.4c00354
ACS EST Engg. XXXX, XXX, XXX−XXX

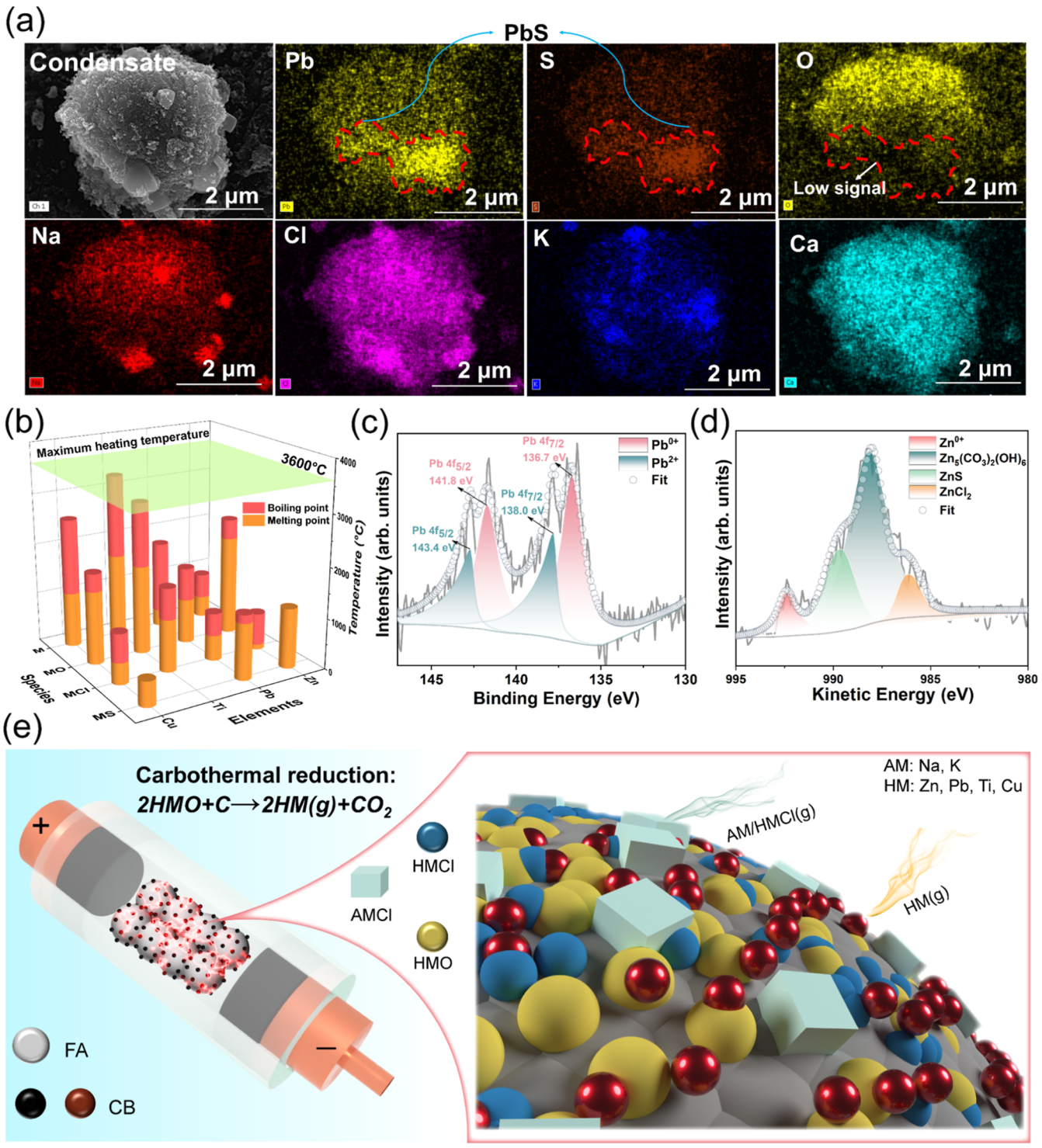


**Figure 6.** Analysis of the morphology of condensate and volatilization mechanism of heavy metals. (a) SEM image of the collected solids, and EDS maps of Pb, S, O, Na, K, Ca, and Cl. Scale bar in SEM image, 2 $\mu$m; scale bars in EDS maps, 2 $\mu$m. (b) Melting and boiling points of Zn, Pb, Ti, and Cu in their elemental, oxidized, chlorinated, and sulfurized states. (c) Pb X-ray photoemission spectroscopy (XPS) fine spectrum of the condensate generated by the initial voltage of 120 V. (d) Zn LMM Auger spectra of the condensate generated by the initial voltage of 120 V. (e) Mechanism diagram of heavy metals volatilization during ultrafast carbothermal process of FA.

found as the main Pb species by mapping EDS analysis (Figure 6a) and XPS analysis (Figure 6c). In Figure 6a, the red line indicates the overlapping regions of enrichment for Pb and S, and the blue line represents the region enriched in oxygen elements. In addition, $PbCl_2$ cannot be excluded but PbO can (Figure 6a). This is because the region enriched in oxygen elements does not overlap with Pb/S. Therefore, the ultrafast carbothermal process contained the reactions of Pb reduction (eqs 1 and 2) and sulfurization (eqs 3−8 possibly).

Reduction

$$2PbO + C \rightarrow 2Pb + CO \quad (1)$$



https://doi.org/10.1021/acsestengg.4c00354
ACS EST Engg. XXXX, XXX, XXX−XXX

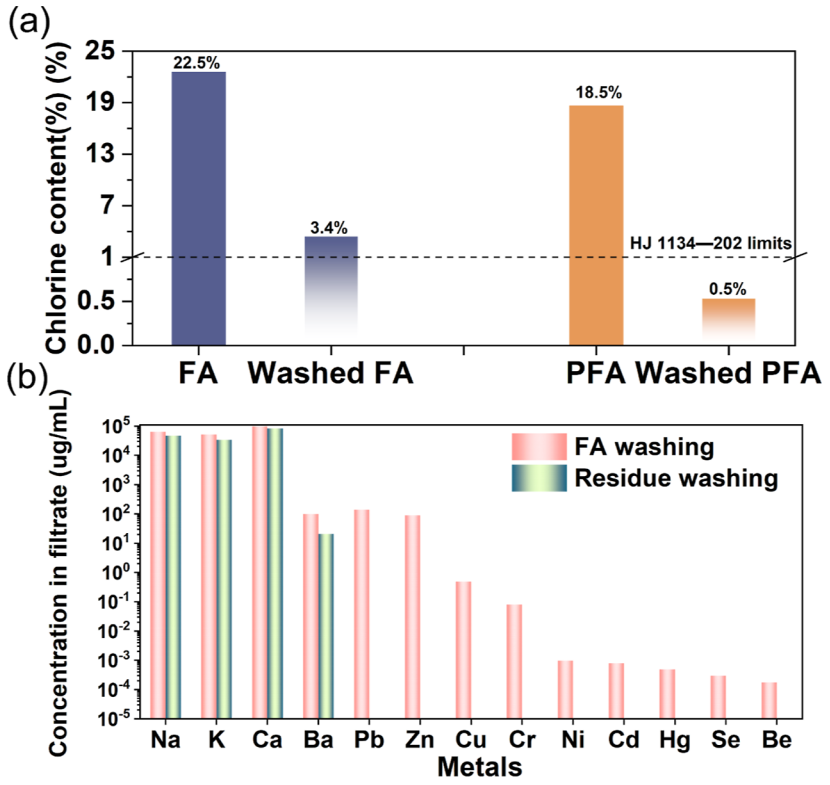


**Figure 7.** Removal effect of chlorine in FA and the ash after the ultrafast carbothermal process (purified fly ash, PFA) by water washing with the liquid−solid ratio of 3:1 L/g. (a) Chlorine content of FA and PFA. (b) Metal concentrations in the filtrate of FA washing and PFA washing.

$$PbO + CO \rightarrow 2Pb + CO_2 \quad (2)$$

Sulfurization

$$CaSO_4 + 4C \rightarrow CaS + 4CO \quad (3)$$

$$2CaClOH \rightarrow Ca(OH)_2 + CaCl_2 \quad (4)$$

$$Ca(OH)_2 \rightarrow CaO + H_2O \quad (5)$$

$$CaS + 2H_2O \rightarrow Ca(OH)_2 + H_2S \quad (6)$$

$$PbO + H_2S \rightarrow PbS + H_2O \quad (7)$$

$$Pb + H_2S(g) \rightarrow PbS + H_2 \quad (8)$$

After three heating cycles, the recovery rate of Zn was 70%, lower than that of Pb 85.3%. This is because the Zn in FA exhibited greater complexity than Pb, involving volatile $ZnCl_2$ (m.p.: 290 °C and b.p.: 732 °C) and less volatile ZnO (m.p.: 1975 °C and b.p.: 2360 °C), $ZnFe_2O_3$, $ZnSiO_4$, and $ZnAl_3O_4$.[31] The $ZnCl_2$ directly evaporates during the heating process. Less volatile ZnO was reduced to elemental Zn (eqs 9 and 10, Figure 6e) through the carbothermal process, which promoted the volatilization of Zn. Additionally, some ZnO reacts with $H_2S$ to produce ZnS (eqs 11 and 12). In the condensate, ZnS, elemental Zn, $ZnCl_2$, and $Zn_5(CO_3)_2(OH)_6$ were found as the main Zn species by Zn LMM Auger spectra (Figure 6d). Therefore, the ultrafast carbothermal process contained the processes of Zn reduction and sulfurization.

$$2ZnO + C \rightarrow 2Zn + CO \quad (9)$$

$$ZnO + CO \rightarrow Zn + CO_2 \quad (10)$$

$$ZnO + H_2S \rightarrow ZnS + H_2O \quad (11)$$

$$Zn + H_2S \rightarrow ZnS + H_2 \quad (12)$$

The dominant Cu species in FA were mainly $CuCl_2$ (m.p.: 620 °C and b.p.: 993 °C), CuO (m.p.: 1450 °C and b. p.: 2000 °C), and $CuSO_4$ (decomposing into CuO at 650 °C).[31] Since the content of Cu and Ti in the condensate was too low to be detected (Figure S5), it was failed to investigate the migration mechanisms through experiments. He et al.[32] found less than 20% of Cu was evaporated for the production of elemental Cu (m.p.: 1084 °C) during the carbothermal treatment of FA at 1000 °C for 2 h in a $N_2$ atmosphere. In this paper, the ultrafast carbothermal process with 3 times heating recovered 64% of Cu, much better than the conventional carbothermal treatment, because the maximum heating temperature was 3600 °C, much higher than the boiling point of elemental Cu of 2567 °C. Other species of Cu have lower melting and boiling points (Figure 6b), making them more easily subjected to volatilization.

The dominant Ti species in FA were not reported, so only some theoretical analyses can be conducted. Elemental Ti (m.p.: 1668 °C and b.p.: 3287 °C) and $TiO_2$ (m.p.: 1850 °C and b. p.: 3000 °C) have much higher melting point and boiling point than $TiCl_3$ (m.p.: 440 °C and b.p.: 960 °C), so $TiCl_3$ should not be the dominant species in FA. In the form of elemental and oxide species, Ti has much higher melting point and boiling point than Zn, Pb, Cu (Figure 6b), so its recovery rate was the lowest (23.6%) among four valuable elements after three times heating. The inability to recycle Ti in previous studies is due to the temperature limitation of the traditional heating devices.

**3.6. Effect of the Ultrafast Carbothermal Process on Chlorine Removal by Water Washing.** In the Technical Specification for Pollution Control of Fly-Ash from MSW


https://doi.org/10.1021/acsestengg.4c00354
ACS EST Engg. XXXX, XXX, XXX−XXX

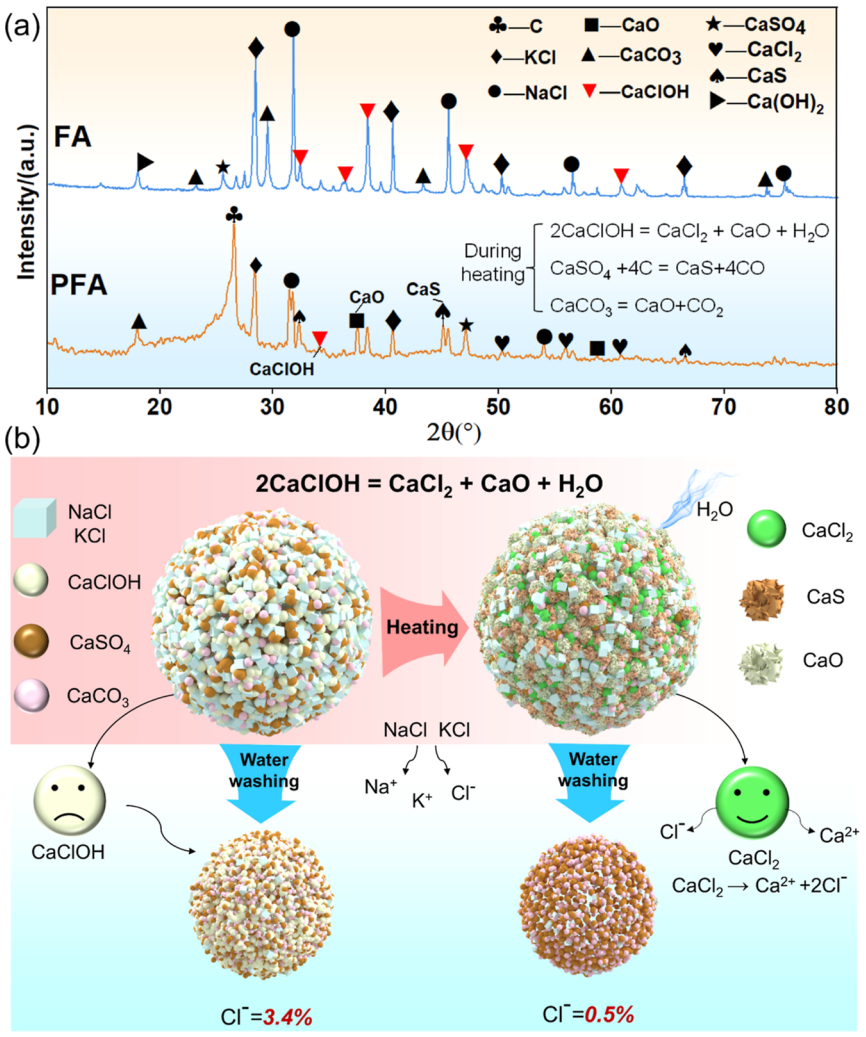


**Figure 8.** Decomposition mechanism of chloride salts in the ultrafast carbothermal process. (a) XRD patterns of FA and PFA. (b) Illustration of the mechanism by which the ultrafast carbothermal process enhances the dissolution of chlorine in FA during the washing process.

incineration (HJ 1134-2020), it is stipulated that the soluble chloride content in FA used for the production of cement clinker should not exceed 2%, ideally lower than 1%. The ultrafast carbothermal process lowered the chlorine content from 22.5% to 18.5%, which is still much higher than 1%, so the additional process was needed to remove chlorides from the residual of the ultrafast carbothermal process. Water washing is an effective method because most chlorides in FA are water-soluble and it is the only method that has already been applied in industry.

As shown in Figure 7a, water washing lowered the chlorine content of FA from 22.6% to 3.4%, higher than the limitation of 1%, so multiple times of washing was need. In contrast, one time of washing was enough for the residual after the ultrafast carbothermal process where the chlorine content was lower to 0.5% (Figure 7a). Therefore, ultrafast carbothermal process improved the dechlorination effect of the water washing process.

Not only chlorides but also heavy metals were dissolved in the water during washing, increasing the difficulty of the washing filtrate treatment for chlorides extraction.[35−37] The filtrate of purified fly ash washing was almost free from heavy metals, except barium (Figure 7b). In addition, the concentrations of sodium and potassium were not reduced significantly. Consequently, the production of NaCl and KCl from filtrate would not be affected, and their cost would be lower and quality would be higher because they were from the salt solution almost free from heavy metals.

**3.7. Mechanism of the Ultrafast Carbothermal Process Promoting Chloride Salts Dissolution in the FA Water Washing Process.** The main components in FA (Figure 8a) are calcium salts (CaClOH, $CaSO_4$, $CaCO_3$) and chloride (NaCl, KCl). Chlorides in the MSWI FA were mainly the species NaCl, KCl, and CaClOH. Zhao et al. utilized a $CO_2$ bubbling washing process to remove chlorine from the FA. They found that NaCl and KCl could be effectively removed, but CaClOH was not as efficiently eliminated.[38] Therefore, the dissolution of CaClOH is more difficult than that of NaCl and KCl during the washing process. It is considered to be the key step in the dissolution of chlorides in the MSWI FA.

After the ultrafast carbothermal process, the chlorine content in FA decreased from 22.5% to 18.5% (Figure 7a), indicating that the ultrafast carbon thermal process did not significantly remove chlorine. However, compared with direct water washing, after the ultrafast carbothermal process, the chlorine content in FA can be reduced from 3.4% to 0.5% by further water washing, suggesting that the ultrafast carbothermal process may have decomposed CaClOH. The XRD patterns


https://doi.org/10.1021/acsestengg.4c00354
ACS EST Engg. XXXX, XXX, XXX−XXX

Table 1. Comparison of Energy Consumption between Ultrafast Carbothermal Process and Lab-Scale Tubular Furnace

| thermal treatment methods | waste | reactor | energy consumption kW h/ton | heating time s | heating temperature °C |
|---|---|---|---|---|---|
| lab-scale ultrafast carbothermal process | FA | FJH | 4917 | 0.3 | max 3600 |
| expected industry ultrafast carbothermal process | FA | FJH | 2947 | 0.15 | max 3600 |
| lab-scale carbothermal treatment | FA | HTF[a] | 296,000 | 7200 | 1000 |
| lab-scale thermal treatment | PCB[b] | HTF[a] | 500,000 | 18,000 | 920 |

[a]Horizontal tube furnace. [b]Printed circuit board.

(Figure 8a) show a significant reduction in the peak of CaClOH, and the appearance of peaks for CaO and $CaCl_2$, confirming that CaClOH in FA decomposes into water-soluble $CaCl_2$ and CaO at high temperatures (Figure 8b). In washing with a low liquid-to-solid ratio, CaClOH is considered to be semidissolved, so after the ultrafast carbothermal process, more chlorine dissolved in the water, promoting the removal of chlorine.

**3.8. Analysis of Energy Consumption and Reactor Size.** Although the maximum temperature reached 3600 °C, the heating time was only 0.3 s, so the energy consumption of the ultrafast carbothermal process was still low. In addition, the sample was self-heated instead of being heated by an external heat source, resulting in low heat loss and high heating efficiency. As shown in Table 1, the energy consumption of ultrafast carbothermal process was 4917 kW h/ton, only 1/110 and 1/188 of the energy consumptions of traditional carbothermal/thermal treatment reported by He et al.[32] and Balaji et al.[41] The detailed calculation of energy consumption during the ultrafast carbothermal process is shown in Text S9.

Furthermore, the industrial energy consumption of ultrafast carbothermal process is expected as 2947 kW h/ton (Text S9). Because the time of the ultrafast carbothermal process is less than one s and that of traditional thermal treatment is more than one h, the volume of FJH reactor could be much smaller than that of a rotary kiln at the same capacity, estimated to be only 1/1920 (Table S4). Therefore, the ultrafast carbothermal process has significant advantages in energy consumption and reactor size. Additionally, our preliminary design for the industrialization of Joule heating features a six-tube linkage system, where two tubes and two sets of reactors discharge simultaneously. Detailed information can be found in Text S15 and Figure S6. This study primarily aims to demonstrate a low-energy, highly efficient method for removing heavy metals and dioxins from FA; therefore, only energy consumption was investigated. The total cost is not calculated because many consumable materials in laboratory-scale experiments are expensive and are expected to be replaced by cheaper materials. The detailed discussion is shown in Text S11.

## 4. CONCLUSIONS

Municipal solid waste incineration fly ash (MSWI FA) is classified as hazardous waste[39,40] for heavy metals[42−46] and dioxins inside. Thermal treatment[47−49] is the promising way to purify MSWI FA, but not widely used for high energy consumption and long calcination time. In this work, the ultrafast carbothermal process was proposed as a new thermal process of the MSWI FA for its low energy consumption and ultrafast heating. The mixture of ash and carbon was heated to 3600 °C within 0.03 s under the optimal operating condition (initial voltage = 120 V, FA to CB mass ratio = 2:1, and initial resistance = 0.78 Ω), which was interpreted by the theoretical calculations. After three times of ultrafast heating, the removal efficiencies of Zn, Pb, Cu, As, Cd, Ni, and Hg were up to 72%, 86%, 71%, 62%, 93%, 70%, and 100%, respectively, the removal efficiency of dioxins was 99.91%, and the purified ash met the leaching standards. The ultrafast carbothermal process also promoted chlorine removal by the ash washing process due to the decomposition of CaClOH in FA at high temperature. The concentrations of valuable Zn, Pb, Ti, and Cu in the condensate of volatiles were 25%, 11%, 2.5%, and 4.1%, respectively, higher than the minimum industrial grade of ore deposit, so these valuable elements have a good recovery value. Compared with the traditional carbothermal treatment, the ultrafast carbothermal process here consumed only 1/110 of energy and needed 1/1920 of the furnace volume.

## ■ ASSOCIATED CONTENT

### Supporting Information

The Supporting Information is available free of charge at https://pubs.acs.org/doi/10.1021/acsestengg.4c00354.

Chemicals and reagents; water washing experiments; analysis of leaching toxicity and PCDDs/DFs; characterizations of FA and residue; analysis of heavy metals; calculation of the theoretical optimal resistance during the heating; calculation of removal and recovery efficiency; energy consumption and cost evaluation; recovery of Zn, Pb, and Cu from condensates; condensate collection system in industrial applications; protective effect of carbon powder on copper electrodes; calculation of volume proportion for the reaction between the glass tube and the sample; methods for collecting the residue and condensate; steps to implement multiple heating cycles include charging, discharging, and adjusting the resistance; relationship between resistance and temperature; reason for not further analyzing the mechanism of dioxin removal in this study; temperatures at three mass ratios and initial voltage 120 V during the whole heating stage; recovery efficiencies of the other heavy metals in FA; recovery efficiencies of heavy metals with the mass ratio of FA to CB, 3:1 and 1:1; Auger spectra of the condensate generated by the initial voltage of 120 V; Industrial design of FJH reactor; relationship between actual resistance, optimal resistance, and temperature; copper electrode after the ultrafast carbon thermal process; condensate collection system in industrial applications; mass balance of the elements between condensate and residue; quartz glass tube after the heating; multiple heating steps; leaching concentrations of heavy metals in FA; detailed concentration changes of various dioxin substances in ash before and after ultrafast carbothermal treatment; real-time voltage changes during the heating process; comparison of reactor size between FJH and rotary kiln; and metal element content in MSWI FA (PDF)


https://doi.org/10.1021/acsestengg.4c00354
ACS EST Engg. XXXX, XXX, XXX−XXX

## AUTHOR INFORMATION


### Corresponding Authors

**Xinye Wang** − *Jiangsu Provincial Key Laboratory of Materials Cycling and Pollution Control, School of Energy and Mechanical Engineering, Nanjing Normal University, Nanjing 210023 Jiangsu, China; Zhenjiang Institute for Innovation and Development, Nanjing Normal University, Zhenjiang 212016 Jiangsu, China;* orcid.org/0000-0002-5084-8849; Email: xinye.wang@njnu.edu.cn

**Haining Meng** − *Everbright Environmental Protection Technology & Equipment (Changzhou) Limited, Changzhou 213100 Jiangsu, China*; Email: menghaining_zribs@163.com

### Authors

**Tengfei Zheng** − *Jiangsu Provincial Key Laboratory of Materials Cycling and Pollution Control, School of Energy and Mechanical Engineering, Nanjing Normal University, Nanjing 210023 Jiangsu, China*

**Huizhen Wang** − *Jiangsu Provincial Key Laboratory of Materials Cycling and Pollution Control, School of Energy and Mechanical Engineering, Nanjing Normal University, Nanjing 210023 Jiangsu, China*

**Rencheng Zhou** − *Jiangsu Provincial Key Laboratory of Materials Cycling and Pollution Control, School of Energy and Mechanical Engineering, Nanjing Normal University, Nanjing 210023 Jiangsu, China*

**Changqi Liu** − *Jiangsu Provincial Key Laboratory of Materials Cycling and Pollution Control, School of Energy and Mechanical Engineering, Nanjing Normal University, Nanjing 210023 Jiangsu, China*

**Hao Xie** − *Jiangsu Provincial Key Laboratory of Materials Cycling and Pollution Control, School of Energy and Mechanical Engineering, Nanjing Normal University, Nanjing 210023 Jiangsu, China; Zhenjiang Institute for Innovation and Development, Nanjing Normal University, Zhenjiang 212016 Jiangsu, China*

**Feifei Zhou** − *Zhenjiang Architectural Science Research Institute, Zhenjiang 212016 Jiangsu, China*

Complete contact information is available at: https://pubs.acs.org/10.1021/acsestengg.4c00354


### Author Contributions

Tengfei Zheng: Investigation, Methodology, Visualization, Writing—original draft, Writing—review and editing. Huizhen Wang: Resources, Investigation, Data curation. Rencheng Zhou: Investigation, Data curation. Changqi Liu: Investigation, Data curation. Hao Xie: Data curation. Feifei Zhou: Data curation. Xinye Wang: Methodology, Supervision, Funding acquisition, Writing—review and editing. Haining Meng: Methodology, Supervision, Funding acquisition, Writing—review and editing. CRediT: **Tengfei Zheng** investigation, methodology, visualization, writing - original draft, writing - review & editing; **Huizhen Wang** data curation, investigation, resources; **Rencheng Zhou** data curation, investigation; **Xinye Wang** funding acquisition, methodology, supervision, writing - review & editing; **Changqi Liu** data curation, investigation; **Hao Xie** data curation; **Feifei Zhou** data curation; **Haining Meng** funding acquisition, methodology, supervision, writing - review & editing.

### Notes

The authors declare no competing financial interest.

## ACKNOWLEDGMENTS

This study was financially supported by the National Natural Science Foundation of China (no.52176115) and the Key Research and Development Program of Zhenjiang City (no. SH2023112).

## REFERENCES


(1) Leckner, B. Process aspects in combustion and gasification Waste-to-Energy (WtE) units. *Waste Manage.* **2015**, *37*, 13−25.

(2) MSW was incinerated in China in 2021. https://www.stats.gov.cn/sj/ndsj/2021/indexeh.htm (accessed March 11, 2024).

(3) MSW was incinerated in Japan in 2021. https://www.env.go.jp/en/press/press_02631.html (accessed March 11, 2024).

(4) MSW was incinerated in European Union in 2021. https://ec.europa.eu/eurostat/web/waste/overview (accessed March 11, 2024).

(5) MSW was incinerated in United States in 2021. https://www.epa.gov/facts-and-figures-about-materials-waste-and-recycling/national-overview-facts-and-figures-materials (accessed March 11, 2024).

(6) Bosio, A.; Zacco, A.; Borgese, L.; Rodella, N.; Colombi, P.; Benassi, L.; Depero, L. E.; Bontempi, E. A sustainable technology for Pb and Zn stabilization based on the use of only waste materials: A green chemistry approach to avoid chemicals and promote CO2 sequestration. *Chem. Eng. J.* **2014**, *253*, 377−384.

(7) González, I.; Vázquez, M. A.; Romero-Baena, A. J.; Barba-Brioso, C. Stabilization of fly ash using cementing bacteria. Assessment of cementation and trace element mobilization. *J. Hazard. Mater.* **2017**, *321*, 316−325.

(8) Huang, T.; Liu, L.; Zhou, L.; Yang, K. Operating optimization for the heavy metal removal from the municipal solid waste incineration fly ashes in the three-dimensional electrokinetics. *Chemosphere* **2018**, *204*, 294−302.

(9) Luo, Z.; Chen, L.; Zhang, M.; Liu, L.; Zhao, J.; Mu, Y. Analysis of melting reconstruction treatment and cement solidification on ultra-risk municipal solid waste incinerator fly ash−blast furnace slag mixtures. *Environ. Sci. Pollut. Res.* **2020**, *27* (25), 32139−32151.

(10) Ma, W.; Chen, D.; Pan, M.; Gu, T.; Zhong, L.; Chen, G.; Yan, B.; Cheng, Z. Performance of chemical chelating agent stabilization and cement solidification on heavy metals in MSWI fly ash: A comparative study. *J. Environ. Manage.* **2019**, *247*, 169−177.

(11) Wang, F.-H.; Zhang, F.; Chen, Y.-J.; Gao, J.; Zhao, B. A comparative study on the heavy metal solidification/stabilization performance of four chemical solidifying agents in municipal solid waste incineration fly ash. *J. Hazard. Mater.* **2015**, *300*, 451−458.

(12) Du, B.; Li, J.; Fang, W.; Liu, J. Comparison of long-term stability under natural ageing between cement solidified and chelator-stabilised MSWI fly ash. *Environ. Pollut.* **2019**, *250*, 68−78.

(13) Wu, K.; Shi, H.; Guo, X. Utilization of municipal solid waste incineration fly ash for sulfoaluminate cement clinker production. *Waste Manage.* **2011**, *31* (9−10), 2001−2008.

(14) Wei, Y.; Liu, S.; Yao, R.; Chen, S.; Gao, J.; Shimaoka, T. Removal of harmful components from MSWI fly ash as a pretreatment approach to enhance waste recycling. *Waste Manage.* **2022**, *150*, 110−121.

(15) Chen, J.; Zhu, W.; Shen, Y.; Fu, C.; Li, M.; Lin, X.; Li, X.; Yan, J. Resource utilization of ultrasonic carbonated MSWI fly ash as cement aggregates: Compressive strength, heavy metal immobilization, and environmental-economic analysis. *Chem. Eng. J.* **2023**, *472*, 144860.

(16) Zhao, X. Y.; Yang, J. Y.; Ning, N.; Yang, Z. S. Chemical stabilization of heavy metals in municipal solid waste incineration fly ash: a review. *Environ. Sci. Pollut. Res. Int.* **2022**, *29* (27), 40384−40402.

(17) Tang, J.; Petranikova, M.; Ekberg, C.; Steenari, B.-M. Mixer-settler system for the recovery of copper and zinc from MSWI fly ash leachates: An evaluation of a hydrometallurgical process. *J. Cleaner Prod.* **2017**, *148*, 595−605.




https://doi.org/10.1021/acsestengg.4c00354
*ACS EST Engg.* XXXX, XXX, XXX−XXX

(18) He, D.; Hu, H.; Jiao, F.; Zuo, W.; Liu, C.; Xie, H.; Dong, L.; Wang, X. Thermal separation of heavy metals from municipal solid waste incineration fly ash: A review. *Chem. Eng. J.* **2023**, *467*, 143344.
(19) Luan, J.; Li, R.; Zhang, Z.; Li, Y.; Zhao, Y. Influence of chlorine, sulfur and phosphorus on the volatilization behavior of heavy metals during sewage sludge thermal treatment. Waste management & research: the journal of the International Solid Wastes and Public Cleansing Association. *Waste Manage. Res.* **2013**, *31* (10), 1012−1018.
(20) Chan, C.; Jia, C. Q.; Graydon, J. W.; Kirk, D. W. The behaviour of selected heavy metals in MSW incineration electrostatic precipitator ash during roasting with chlorination agents. *J. Hazard. Mater.* **1996**, *50* (1), 1−13.
(21) Kumagai, S.; Hirahashi, S.; Grause, G.; Kameda, T.; Toyoda, H.; Yoshioka, T. Alkaline hydrolysis of PVC-coated PET fibers for simultaneous recycling of PET and PVC. *J. Mater. Cycles Waste Manage.* **2018**, *20* (1), 439−449.
(22) Lane, D. J.; Jokiniemi, J.; Heimonen, M.; Peräniemi, S.; Kinnunen, N. M.; Koponen, H.; Lähde, A.; Karhunen, T.; Nivajärvi, T.; Shurpali, N.; et al. Thermal treatment of municipal solid waste incineration fly ash: Impact of gas atmosphere on the volatility of major, minor, and trace elements. *Waste Manage.* **2020**, *114*, 1−16.
(23) Zeng, C.; Duan, C.; Guo, Z.; Liu, Z.; Dou, S.; Yuan, Q.; Liu, P.; Zhang, J.; Luo, J.; Liu, W.; et al. Ultrafastly activated needle coke as electrode material for supercapacitors. *Prog. Nat. Sci.: Mater. Int.* **2022**, *32* (6), 786−792.
(24) Luo, J.; Zhang, J.; Guo, Z.; Liu, Z.; Dou, S.; Liu, W.-D.; Chen, Y.; Hu, W. Recycle spent graphite to defect-engineered, high-power graphite anode. *Nano Res.* **2023**, *16* (4), 4240−4245.
(25) Cheng, Y.; Chen, J.; Deng, B.; Chen, W.; Silva, K. J.; Eddy, L.; Wu, G.; Chen, Y.; Li, B.; Kittrell, C.; et al. Flash upcycling of waste glass fibre-reinforced plastics to silicon carbide. *Nat Sustainability* **2024**, *7* (4), 452−462.
(26) Deng, B.; Wang, X.; Luong, D. X.; Carter, R. A.; Wang, Z.; Tomson, M. B.; Tour, J. M. Rare earth elements from waste. *Sci. Adv.* **2022**, *8* (6), No. eabm3132.
(27) Deng, B.; Meng, W.; Advincula, P. A.; Eddy, L.; Ucak-Astarlioglu, M. G.; Wyss, K. M.; Chen, W.; Carter, R. A.; Li, G.; Cheng, Y.; et al. Heavy metal removal from coal fly ash for low carbon footprint cement. *Commun. Eng.* **2023**, *2* (1), 13.
(28) Deng, B.; Luong, D. X.; Wang, Z.; Kittrell, C.; McHugh, E. A.; Tour, J. M. Urban mining by flash Joule heating. *Nat. Commun.* **2021**, *12* (1), 5794.
(29) Algozeeb, W. A.; Savas, P. E.; Luong, D. X.; Chen, W.; Kittrell, C.; Bhat, M.; Shahsavari, R.; Tour, J. M. Flash Graphene from Plastic Waste. *ACS Nano* **2020**, *14* (11), 15595−15604.
(30) Chen, Y.; Egan, G. C.; Wan, J.; Zhu, S.; Jacob, R. J.; Zhou, W.; Dai, J.; Wang, Y.; Danner, V. A.; Yao, Y.; et al. Ultra-fast self-assembly and stabilization of reactive nanoparticles in reduced graphene oxide films. *Nat. Commun.* **2016**, *7* (1), 12332.
(31) Cheng, T. W.; Chu, J. P.; Tzeng, C. C.; Chen, Y. S. Treatment and recycling of incinerated ash using thermal plasma technology. *Waste Manage.* **2002**, *22* (5), 485−490.
(32) He, D.; Zhou, F.; Meng, H.; Lu, X.; Xie, H.; Wang, X.; Dong, L. Carbothermal treatment of municipal solid waste incineration fly ash: Purification and valuable elements extraction. *Sep. Purif. Technol.* **2024**, *331*, 125713.
(33) Jakob, A.; Stucki, S.; Kuhn, P. Evaporation of Heavy Metals during the Heat Treatment of Municipal Solid Waste Incinerator Fly Ash. *Environ. Sci. Technol.* **1995**, *29* (9), 2429−2436.
(34) Zhang, J.; Zhang, S.; Liu, B. Degradation technologies and mechanisms of dioxins in municipal solid waste incineration fly ash: A review. *J. Cleaner Prod.* **2020**, *250*, 119507.
(35) Ma, W.; Wenga, T.; Frandsen, F. J.; Yan, B.; Chen, G. The fate of chlorine during MSW incineration: Vaporization, transformation, deposition, corrosion and remedies. *Prog. Energy Combust. Sci.* **2020**, *76*, 100789.
(36) Liu, Z.; Fang, W.; Cai, Z.; Zhang, J.; Yue, Y.; Qian, G. Garbage-classification policy changes characteristics of municipal-solid-waste fly ash in China. *Sci. Total Environ.* **2023**, *857*, 159299.
(37) Wang, Y.; Zhu, H.; Jiang, X.; Lv, G.; Yan, J. Study on the evolution and transformation of Cl during Co-incineration of a mixture of rectification residue and raw meal of a cement kiln. *Waste Manage.* **2019**, *84*, 112−118.
(38) Zuo, W.; Zhao, R.; Dong, G.; Ma, G.; Zhou, H.; Song, T.; Tu, Y.; Xie, H.; Wang, X. CO2-Assisted Water-Washing Process of Municipal Solid Waste Incineration Fly Ash for Chloride Removal. *Energy Fuels* **2022**, *36* (22), 13732−13742.
(39) Rissler, J.; Klementiev, K.; Dahl, J.; Steenari, B. M.; Edo, M. Identification and Quantification of Chemical Forms of Cu and Zn in MSWI Ashes Using XANES. *Energy Fuels* **2020**, *34* (11), 14505−14514.
(40) Wang, H.; Zhao, B.; Zhu, F.; Chen, Q.; Zhou, T.; Wang, Y. Study on the reduction of chlorine and heavy metals in municipal solid waste incineration fly ash by organic acid and microwave treatment and the variation of environmental risk of heavy metals. *Sci. Total Environ.* **2023**, *870*, 161929.
(41) Balaji, R.; Senophiyah-Mary, J. A Comparative Study on the Cost−Benefit Analysis on Metal Recovery of WPCB Using Pyrometallurgy with Two Different Thermal Furnaces. In *Urban Mining and Sustainable Waste Management*; Ghosh, S. K., Ed.; Springer Singapore, 2020; pp 59−67.
(42) Wu, B.; Wu, J.; Li, J.; Qiao, Z.; Shen, P.; Zhang, Q.; Zhang, B.; Ling, Y. Heterostructure $\alpha$-Fe2O3(001)/g-C3N4(002) adsorbent to remove $As_2O_3$ in simulated coal flue gas: Experimental and DFT study. *Chem. Eng. J.* **2023**, *471*, 144575.
(43) Zhang, X.; Zhang, B.; Zhang, Q.; Wu, J.; Ye, L.; Li, S.; Ling, Y.; Luo, G.; Yao, H.; Wu, B. Fe-Ni bimetallic adsorbent for efficient $As_2O_3$ removal from coal-fired flue gas under a wide temperature range: Experimental and DFT study. *Fuel* **2024**, *357*, 129803.
(44) Xue, Y.; Fang, X.; Jiang, H.; Wu, J.; Liu, H.; Li, X.; He, P.; Li, F.; Qi, Y.; Gao, Q.; et al. Hierarchical microsphere Flower-like SnIn4S8 with active sulfur sites for adsorption and removal of mercury from coal-fired flue gas. *Chem. Eng. J.* **2023**, *472*, 145105.
(45) Chen, L.; Li, C.; Zhao, Y.; Wu, J.; Li, X.; Qiao, Z.; He, P.; Qi, X.; Liu, Z.; Wei, G. Constructing 3D Bi/$Bi_4O_5I_2$ microspheres with rich oxygen vacancies by one-pot solvothermal method for enhancing photocatalytic activity on mercury removal. *Chem. Eng. J.* **2021**, *425*, 131599.
(46) Qiao, Z.; Chu, W.; Zhou, H.; Peng, C.; Guan, Z.; Wu, J.; Yoriya, S.; He, P.; Zhang, H.; Qi, Y. Construction of Z scheme S-g-$C_3N_4$/$Bi_5O_7I$ photocatalysts for enhanced photocatalytic removal of Hg0 and carrier separation. *Sci. Total Environ.* **2023**, *872*, 162309.
(47) Dong, L.; Wang, L.; Wen, H.; Lin, Z.; Yao, Z.; Zou, C.; Xu, H.; Hu, H.; Yao, H. Numerical investigation of the oxy-fuel combustion in the fluidized bed using macroscopic model supported by CFD-DDPM. *J. Environ. Chem. Eng.* **2024**, *12* (5), 113959.
(48) Zhu, Z.; Huang, Y.; dong, L.; Xu, W.; Yu, M.; Li, Z.; Xiao, Y.; Cheng, H. Dual effects of NaCl on the high temperature adsorption of heavy metals by montmorillonite. *Chem. Eng. J.* **2024**, *494*, 152661.
(49) Zhu, Z.; Huang, Y.; dong, L.; Yu, M.; Xu, W.; Li, Z.; Xiao, Y.; Cheng, H. Effect of aluminosilicates on the release and form transformation of semi-volatile heavy metals during the combustion of hyperaccumulator plants. *J. Cleaner Prod.* **2024**, *461*, 142604.


https://doi.org/10.1021/acsestengg.4c00354
*ACS EST Engg.* XXXX, XXX, XXX−XXX